HHS Public Access

Author manuscript

Toxicol Appl Pharmacol. Author manuscript; available in PMC 2016 November 15.

Published in final edited form as:

Toxicol Appl Pharmacol. 2015 November 15; 289(1): 58–69. doi:10.1016/j.taap.2015.09.002.

A fetal whole ovarian culture model for the evaluation of CrVI-induced developmental toxicity during germ cell nest breakdown

Jone A. Stanley, **Joe A. Arosh**, **Robert C. Burghardt**, and **Sakhila K. Banu***

Department of Veterinary Integrative Biosciences, College of Veterinary Medicine and Biomedical Sciences, Texas A&M University, College Station, TX 77843, USA

Abstract

Prenatal exposure to endocrine disrupting chemicals (EDCs), including bisphenol A, dioxin, pesticides, and cigarette smoke, has been linked to several ovarian diseases such as premature ovarian failure (POF) and early menopause in women. Hexavalent chromium (CrVI), one of the more toxic heavy metals, is widely used in more than 50 industries. As one of the world's leading producers of Cr compounds, the U.S. is facing growing challenges in protecting human health against adverse effects of CrVI. Our recent findings demonstrated that *in vivo* CrVI exposure during gestational period caused POF in F1 offspring. Our current research focus is *three-fold*: (i) to identify the effect of CrVI on critical windows of great vulnerability of fetal ovarian development; (ii) to understand the molecular mechanism of CrVI-induced POF; (iii) to identify potential intervention strategies to mitigate or inhibit CrVI effects. In order to accomplish these goals we used a fetal whole ovarian culture system. Fetuses were removed from the normal pregnant rats on gestational day 13.5. Fetal ovaries were cultured *in vitro* for 12 days, and treated with or without 0.1 ppm potassium dichromate (CrVI) from culture day 2-8, which recapitulated embryonic day 14.5 – 20.5, *in vivo*. Results showed that CrVI increased germ cell/oocyte apoptosis by increasing caspase 3, BAX, p53 and PUMA; decreasing BCL2, BMP15, GDF9 and cKIT; and altering cell cycle regulatory genes and proteins. This model system may serve as a potential tool for high throughput testing of various drugs and/or EDCs in particular to assess developmental toxicity of the ovary.

Keywords

fetal ovary; chromium; germ cell; apoptosis

* ***Address correspondence to***: **Sakhila K. Banu**, Department of Integrative Biosciences, College of Veterinary Medicine and Biomedical Sciences, Texas A&M University, College Station, Texas 77843, USA, Phone: 979-458-3613, Fax: 979-847-8981, skbanu@cvm.tamu.edu.

Disclosure Statement: The authors have nothing to disclose.

Introduction

Prenatal exposure to endocrine disrupting chemicals (EDCs), including bisphenol A (BPA) (Wang *et al.*, 2014), dioxin (Shi *et al.*, 2007), pesticides (Armenti *et al.*, 2008), and cigarette smoke (Tawfik *et al.*, 2015), has been linked to several ovarian diseases such as premature ovarian failure (POF) and early menopause in women. Disturbances in the initial steps or processes that facilitate fetal ovarian differentiation result in incomplete sexual development and may contribute to childhood and adult diseases such as gonadal dysgenesis, infertility or ovarian cancer (de Boo and Harding, 2006). Exposure to EDCs lead to a reduced initial primordial follicle pool (Rivera *et al.*, 2011; Manikkam *et al.*, 2014) and/or to accelerated decline in primordial follicle number (Rodríguez *et al.*, 2010; Nilsson *et al.*, 2012). This would ultimately decrease the reproductive lifespan of affected females by reducing the primordial follicle pool below the critical threshold necessary to maintain ovarian activity. Primordial follicles are formed during gestation in humans but after birth in rodents in a process that involves dissolution of germ cell nests (GCN) that form during germ cell mitosis (Pepling, 2006). The process of GCN breakdown involves migration of somatic/pre-granulosa cells into the GCN and simultaneous disruption of the inter-oocyte bridges through apoptosis of individual oocytes (Pepling and Spradling, 1998). The pre-granulosa cells then surround the remaining oocytes to form primordial follicles that constitute the resting stock of gametes for the entire reproductive lifespan of female mammals (Pepling, 2006). Thus, any alteration in this process and/or timing might lead to a reduced primordial follicle pool size, resulting in POF and infertility.

In the developing rodent ovary, germ cell apoptosis occurs at all stages of oogenesis with two main waves: the *first wave* of cell death coincides with the entry of oogonia into meiosis (E13.5–15.5); and the *second wave* occurs between E17.5 and postnatal day (PND) 1, marking the GCN breakdown and the beginning of primordial follicle assembly (Coucouvanis *et al.*, 1993; Ratts *et al.*, 1995). In rats, primordial follicle assembly is initiated neonatally and continues for 3–4 days (Rajah *et al.*, 1992), where apoptosis plays a key role in the entire process (Pepling and Spradling, 2001; Sawyer *et al.*, 2002). The key triggers and mediators of apoptosis responsible for massive germ cell death during this period are not known and the underlying physiological reasons for this loss are still unclear (Myers *et al.*, 2014). Our previous findings identified a role for p53 pathway in hexavalent chromium (CrVI)-induced germ cell (Sivakumar *et al.*, 2014) and granulosa cell (Banu *et al.*, 2011) apoptosis. Activation of p53 leads to cell growth arrest, senescence or apoptosis (Yamakuchi and Lowenstein, 2009). In addition, p53 is directly translocated to mitochondria and forms complexes with the BCLXL and BCL2 proteins, increases permeabilization of the outer mitochondrial membrane, facilitates release of cytochrome c, activates caspase 3 to induce apoptosis (Haupt *et al.*, 2003a; Haupt *et al.*, 2003b). When cells are exposed to oxidative stress, toxicants, DNA damage and hypoxia signals, p53 protein is stabilized, activated and transported into nucleus and induces apoptosis (Giaccia and Kastan, 1998).

Growth differentiation factor 9 (GDF9), bone morphogenetic protein 15 (BMP15) and cKIT play crucial roles in follicular development and oocyte maturation (Thomas and Vanderhyden, 2006). There is compelling evidence in several mammalian species that GDF9 is essential for early stages of follicle development (Dong *et al.*, 1996) and BMP15 is

essential for late stages of follicle development (Otsuka *et al.*, 2011). GDF9 promotes follicular survival by suppressing granulosa cell apoptosis and follicular atresia (Orisaka *et al.*, 2006). Combined mutation of *Bmp15* and *Gdf9* lead to multi oocyte follicles in mouse (Yan *et al.*, 2001). In the human, mutations in both these genes have been associated with POF (Dixit *et al.*, 2005; Dixit *et al.*, 2006). Interestingly, our recent findings indicate that CrVI exposure during prenatal development caused POF in F1 progeny (Sivakumar *et al.*, 2014) and altered the spatiotemporal expression pattern of Xpnpep2 in fetal ovaries. XPNPEP2 is a candidate protein for POF in women (Prueitt *et al.*, 2000).

Major limitations in understanding the direct effects of EDCs on ovarian cellular dynamics in mammals, including humans, include a lack of proper and simple tools/techniques as well as gaps in knowledge regarding the critical window(s) of vulnerability. Identifying such tools and evaluating the effects of EDCs on cellular dynamics during the critical windows of ovarian development will be helpful in: (i) high throughput toxicity screening and/or testing of EDCs; (ii) identifying the specific effects of various EDCs on follicle development; and (iii) dissecting the critical window(s) of vulnerability and key mechanisms/pathways involved in such window(s). The first paper in the literature on the *in vitro* culture of fetal ovaries (embryonic day (E) 16) was published in 1938 by Martinovitch (Martinovitch, 1938); followed by Blandau et al., 1965 (Blandau *et al.*, 1965), and Motohashi et al., in 2009 (Motohashi *et al.*, 2009). By refining these previous protocols, including the *in vitro* whole ovarian culture from neonatal rodents developed in the Hoyer lab (Devine *et al.*, 2002), we assessed immunohistochemical localization of pro-apoptotic, anti-apoptotic, and oocyte-specific protein machinery, and mRNA and protein expression pattern of cell cycle regulatory machinery in a fetal whole ovarian culture system.

Significant contamination with CrVI has been found in the drinking water sources of more than 30 cities in the U.S. (Sutton, 2010), with a highest chromium (Cr) level in drinking water source in Midland, TX of 5.28 mg/L or 5.28 ppm. This is 52.8 times greater than the regulatory dose of Cr in drinking water (0.1 ppm). Previous epidemiological studies have reported an increase in the risk of spontaneous abortion among women employed in Finnish metal industries (Hemminki *et al.*, 1980; Hemminki *et al.*, 1983). Welding fumes and metal dusts containing CrVI are known to be either teratogenic, carcinogenic, embryotoxic or mutagenic (Stern *et al.*, 1986; Quansah and Jaakkola, 2009). Occupational exposure to Cr during pregnancy increased the rate of abortion (Yang *et al.*, 2013), decreased intrauterine growth of the fetuses, resulting in low birth weight of the new born children (Quansah and Jaakkola, 2009). The effect of CrVI on the course of pregnancy and childbirth were studied in women employees at a dichromate manufacturing facility in Russia (Shmitova, 1980). These women had high levels of Cr in blood and urine and they experienced gynecological illnesses, abortion, postnatal hemorrhage and birth complications. They had Cr levels in the umbilical cord blood of 0.27 ± 0.005 mg/L, 0.24 ± 0.047 mg/L, and 0.1 ± 0.021 mg/L at 12, 32 and 40 weeks of gestation, respectively. Likewise, Cr levels in urine samples from these women ranged from 0.043 – 0.1 mg/L (Shmitova, 1980). Another study from Guiyu, China (Li *et al.*, 2008) showed increased Cr levels in umbilical cord blood from neonates born to the women who were occupationally exposed to Cr at electronic waste recycling sites. In this study, the authors documented umbilical cord blood (UCB) Cr levels in neonates from

0.00045 – 6.0 mg/L, with an average mean concentration of Cr 0.3 mg/L. There is a positive correlation between Cr levels in UCB and Cr-induced DNA damage of UCB lymphocytes. Increased levels of Cr in the blood and urine of chrome plating workers is associated with elevated levels of free radicals and chromosomal aberrations (Maeng *et al.*, 2004). The objective of the current investigation was to determine the effect of *in vitro* exposure to 0.1 mg/L or 0.1 ppm during germ cell apoptosis (E13.5 - 20.5), GCN breakdown and primordial follicle assembly on apoptotic pathways and follicle atresia. This dose is within the range of reported Cr levels in UCB or urine in women exposed to CrVI and is also a regulatory dose of Cr in drinking water in the U.S (USEPA, 2009).

Materials and methods

Chemicals

The reagents used in this study were purchased from the following suppliers: DNA ladder, TRIzol, antibiotic-antimycotic, trypsin-EDTA (Invitrogen Life Technologies Inc., Carlsbad, CA); one-step reverse transcriptase-polymerase chain reaction (RT-PCR) (Qiagen Inc., Valencia, CA); power SybrGreen PCR master mix (Life Technologies, CA); fetal bovine serum (Hyclone, Logan, UT); and tissue culture dishes and plates (Corning Inc., Corning, NY); potassium dichromate ($K_2Cr_2O_7$) (Sigma-Aldrich, St. Louis, MO). The other chemicals used were molecular biologic grade available from Fisher Scientific (Pittsburgh, PA) or Sigma-Aldrich (St. Louis, MO). All oligonucleotide primers were commercially synthesized by Integrated DNA Technologies Inc., Coralville, Iowa. Details of sources of antibodies, catalog numbers, dilutions, host species, immunogens, and homologies with rat/mouse are given in Table-1.

In vitro culture of the fetal ovary and experimental design

Animal use protocols were approved by the Animal Care and Use Committee of Texas A&M University and were in accordance with the standards established by Guiding Principles in the Use of Animals in Toxicology and Guidelines for the Care and Use of Experimental Animals by the National Institutes of Health and the American Veterinary Medical Association. Normal timed-pregnant rats of 60-70 days of age were euthanized by CO_2 asphyxiation followed by cervical dislocation on 13.5 days *post coitus*. According to the AVMA guidelines (Leary *et al.*, 2013), after confirming the death of the dams, the uteri were quickly cut opened and embryos were immersed (with the amniotic sac intact) in cold (4-8°C/35-39°F) physiological saline in a glass beaker until they became completely immobile. After confirming that the embryos were immobile, amniotic sacs were cut opened, embryos were decapitated with the scissors, and placed under a zoom stereo microscope. The ovaries were removed along with the mesonephros using sterile surgical instruments. Ovaries were carefully placed on top of a sterile membrane floating on the culture media in a 24-well culture plate. A drop of the culture media was placed on top of the ovaries to keep them from drying. Ovaries were cultured in Ham's F-12/DMEM (1:1) media containing 1 mg/ml BSA, 1 mg/ml Albumax, 27.5μg/ml transferrin, 5 U/ml penicillin, and 5 μg/ml streptomycin; and placed in a CO_2 incubator. Embryonic day (E) 13.5 was considered as culture day (CD) 1, and ovaries were cultured for a period of 9 or 12 days, and harvested on CD 9 or 12, which recapitulates postnatal day (PND) 1 and PND 4,

respectively (Fig. 1). According to Environmental Protection Agency (EPA), the maximum contamination level (MCL) or regulatory dose of Cr in the drinking water is 0.1 ppm (0.1 mg/L) (USEPA, 2009). This regulatory dose of CrVI (0.1 ppm potassium dichromate) was used in the current study. CrVI was added to the media from CD 2 through CD 8, every 24 h (E 14.5 - 20.5). As explained earlier, E 14.5 – 20.5 comprises a germ cell breakdown window with germ cells undergoing the first and second waves of apoptosis. On CD 9 (PND1) and 12 (PND4), ovaries were removed for further analyses.

Histology

Histological processing of the ovary was performed by the Histology core lab facility, College of Veterinary Medicine & Biomedical Sciences, Texas A&M University, based on the standard protocols for paraffin-embedded sections that were cut at 5 μm thickness and stained with hematoxylin and eosin (H&E).

TUNEL assay

Paraffin-embedded tissue sections were deparaffinized and TUNEL assay was performed as we described recently (Stanley *et al.*, 2013; Sivakumar *et al.*, 2014; Stanley *et al.*, 2014; Banu *et al.*, 2015). The apoptosis index (AI) was calculated as the average percentage of TUNEL-positive germ cells/oocytes from the ovaries (n=8) at magnification x400.

Histological evaluation of follicular atresia

On CD12 (which recapitulates PND 4), ovaries were collected and serial sections were made. The number of atretic follicles were counted in every 12^{th} section to prevent counting the same follicle more than once (Devine *et al.*, 2002). Briefly, ovaries were fixed processed, serially sectioned (5 μm), and stained with hematoxylin and eosin. Those follicles with intact oocytes were included in the counting. The criteria to identify atretic follicles was according to Osman (Osman, 1985) and Borgeest et al., (Borgeest *et al.*, 2002) as follows: degenerative changes in the granulosa cell layer which shows cell shrinkage, pyknosis, and karyorrhexis and/or degenerative changes in the oocyte such as the breakdown of the nuclear membrane with oocyte fragmentation (Stanley *et al.*, 2014).

Whole mount florescence immunohistochemistry, analysis of germ cell nest breakdown

The whole mount double immunofluorescence staining procedure was followed as we described recently (Banu et al., 2015). In brief, the ovaries were fixed with 5.3% formaldehyde (Cat#18814, Polysciences) overnight at 4°C. After several washings with PBS, they were labeled with primary antibodies overnight at 4°C for both VASA (germ cell marker) and GATA4 (somatic cell marker) at the appropriate dilution (Table 1). The ovaries were incubated with fluorophore-conjugated secondary antibodies, namely, Alexa Fluor® 488 conjugate for VASA (Cat. No. A21121, Invitrogen, NY, USA) and Alexa Fluor 594 conjugate for GATA4 (Cat. No. A11037, Invitrogen, NY, USA) for 4 h at RT, and overlaid with a cover glass and mounting medium containing Prolong Gold® antifade reagent (Life Technologies). Images were obtained on a Zeiss LSM 510 confocal microscope with a plan apochromat 63x/1.4 NA oil objective. For recording the VASA signal, the argon laser set was used at an excitation of 488 nm and emission collected with a BP 500-550 nm. For

recording the GATA signal, a HeNe laser was used at an excitation of 543 nm and emission collected with a long pass filter LP 560 nm. At least ten images were collected per treatment. In order to analyze GCN breakdown, for each ovary, two cores were visualized and counted. A core is a region 135 × 135 μm consisting of optical sections at four different depths in the ovary, each 15–20 μm apart. Thus, for each ovary, two cores were obtained consisting of four optical sections per core for a total of eight optical sections per ovary (Sivakumar et al., 2014). Total number of germ cells were counted in the ovaries from the control group and considered as 100%. Total number of germ cells from the CrVI group was calculated and expressed as the relative number in percentage, compared with control. The number of single oocytes found in the nest relative to the total number of oocytes was determined for each ovary and reported as percent single oocytes.

Immunohistochemistry

Sources of antibodies, catalogue numbers, dilution, host species, immunogen and homology with rat/mouse are given in Table-1. Ovaries were fixed in 4% buffered paraformaldehyde for 1 h at 4°C and processed using standard procedures as described (Sivakumar *et al.*, 2014; Stanley *et al.*, 2014). The tissue sections were incubated with specific primary antibodies at specific concentrations (Table 1). Digital images were captured using a Zeiss Axioplan 2 Research Microscope (Carl Zeiss, Thornwood, NY) with an Axiocam HR digital color camera. The intensity of staining for each protein was quantified using Image-ProPlus 6.3 image processing and analysis software according to the manufacturer's instructions (Media Cybernetics, Inc.; Bethesda, MD). In brief, six images of the ovary at 400x magnification were captured randomly without hot-spot bias in each tissue section per animal. Integrated Optical Density (IOD) of immunostaining was quantified in the RGB mode. Numerical data were expressed as least square mean ± SEM. We also performed conventional blind scoring to count cells with positive staining in order to validate the methods. There was no significant difference between quantifying IOD and blind scoring system (data not shown).

Effects of CrVI on oxidative stress and antioxidant enzymes

Oxidative stress and antioxidant activities were measured from the culture media as we described previously (Stanley *et al.*, 2013). As described for the experimental design, fetal whole ovarian culture was started on E13.5 (CD1), CrVI was added to the media on CD2, and samples of media were collected every 24 hour from CD3 until CD12. LPO levels in the media were measured using a colorimetric measurement kit as per the manufacturer's instruction (Cat. No. 705003, Cayman Chemical, Ann Arbor, MI, USA). The kit measures hydroperoxides directly utilizing the redox reactions with ferrous ions. Briefly, LPO was extracted into chloroform, and directly used in the assay, thus it eliminates any interference caused by H_2O_2 and/or endogenous ferric ions in the sample. Hydroxyperoxides are highly unstable and react with ferrous ions to produce ferric ions. The resulting ferric ions were detected using thiocyanate ion as the chromogen and quantified at 500 nm. GPx was measured using a commercial kit (Cat. No. 703102, Cayman Chemical, Ann Arbor, MI, USA) according to the manufacturer's protocol. SOD was measured using a commercial kit (Cat. No. 706002, Cayman Chemical, Ann Arbor, MI, USA) according to the manufacturer's protocol. The kit utilizes the interaction between hypoxanthine and xanthine oxidase to produce O^{-2} radicals, which are detected using tetrazolium salt and can be read at

460 nm. The kit detects all three types of SOD metalloenzymes: copper/zinc, manganese, and iron. One unit of SOD is defined as the amount of enzyme required to dismutate 50% of the O^{-2} radicals. The catalase activity was measured using a commercial kit (Cat. No. 707002, Cayman Chemical, Ann Arbor, MI, USA). In this assay, catalase reacts with methanol in the presence of H_2O_2 to produce formaldehyde, which is then measured by adding 4-amino-3-hydrazino-5-mercapto-1, 2, 4-triazole to form a purple reaction product that can be detected spectrophotometrically at 540 nm.

Real-Time Reverse Transcription (RT)-Polymerase Chain Reaction (PCR)

Total RNA was isolated using RNeasy Micro Kit (Cat. No. 74004, Qiagen, USA) according to manufacturer's instructions. The purity and concentration of RNA was determined spectrophotometrically by measuring the absorbance at 260/280 nm and a purity of 1.8 - 2.0 was considered acceptable for the real time RT-PCR analysis. The first strand cDNA was synthesized using 100ng total RNA by QuantiTect RT kit (Cat. 205311, Qiagen, USA) according to manufacturer's instructions. Real-time PCR was performed using the Power SYBR®Green master mix (Cat. 4368577, Life Technologies, USA) according to manufacturer's instructions. cDNA (2μl) was mixed with 10μl master mix (dNTP mix, AmpliTaq Gold® DNA polymerase, optimized buffer components and SYBR®Green I dye), sense and anti-sense oligonucleotide primers for respective genes and β-actin gene for internal control, with the total reaction volume made up to 20μl with RNase free water. The reaction cycles were as follows: PCR enzyme initial activation at 95°C for 15 min; initial denaturation at 94°C for 15 sec, annealing at 60°C for 30 sec and elongation at 72°C for 30 sec. All reactions were run in triplicate. The PCR amplification of all transcripts was performed on the Step-One Plus real-time PCR machine (Life Technologies, Carlsbad, CA). The fold differences were calculated by normalizing the relative expression of gene of interest with β-actin and the results expressed as fold changes. Details of the sense and anti-sense oligonucleotide primer sequences used for the real-time PCR analysis were given in Table-2. Relative gene expression was presented by comparative CT (also referred to as the ΔΔCT) method (Schmittgen and Livak, 2008).

Statistical analysis

Effects of CrVI on various parameters in the ovary were analyzed and the results were expressed as mean ± SEM. Student *t*-test was used to compare groups and *P* values less than 0.05 were considered significant.

Results

Effects of CrVI on germ cell death, germ cell nest breakdown and early stages of primordial follicle assembly

On PND1, control ovaries had tightly packed germ cells mostly residing inside the nests, with a very few isolated oocytes surrounded by the pre-granulosa cells in the form of primordial follicles, whereas, CrVI-treated ovaries appeared to have broken GCN with several isolated primordial or early primary follicles (Figs. 2C & I). Several pyknotic nuclei were found in the ovaries (Fig. 2C). Results from in situ TUNEL assay indicated that CrVI increased apoptosis of the oocytes and granulosa cells (Fig. 2D-F). Double immunolabelling

with VASA and GATA4 showed tightly packed germ cells in the control ovaries (both freshly collected from PND1 pups and cultured *in vitro*) (Fig. 2G&H). However, CrVI treatment increased the number of isolated oocytes surrounded by granulosa cells, thus accelerating or advancing primordial follicle assembly and primary follicle transition (Fig. 2L).

Effects of CrVI on atresia of pre-antral follicles

On PND4, CrVI increased oocyte apoptosis (Fig. 3F) and atresia of both primordial and primary follicles compared to control (Figs 3 C, H & I). Several pyknotic bodies and increase in eosinophilic staining were also observed under CrVI treatment (Fig 3 C).

Effects of CrVI on the expression of BCL2, Caspase 3, BAX, p53 and PUMA

Our previous studies on *in utero* exposure to CrVI indicated that CrVI increased germ cell apoptosis through a down regulation of BCL2 and an up regulation of caspase 3, BAX and p53 on PND1 (Sivakumar *et al.*, 2014). In order to confirm if the same mechanism operates under *in vitro* whole ovarian culture, we measured the expression of BCL2, caspase 3, BAX and p53 along with p53 upregulated modulator of apoptosis (PUMA) on PND1 (CD9). CrVI significantly decreased the expression of BCL2, and increased the expression of caspase 3, BAX, p53 and PUMA in the ovary compared to control (Fig 4 A-O).

Effects of CrVI on the expression of oocyte-specific proteins

CrVI down regulated the expression of oocyte specific proteins BMP15, GDF9 and cKIT compared to control on PND1 (CD9) (Fig 5A-I).

Effects of CrVI on oxidative stress and the activity of antioxidant enzymes

In order to determine the effects of CrVI on oxidative stress and antioxidant enzymes, we determined the levels of lipoperoxidase (LPO), an oxidative stress marker, and antioxidant enzymes GPx, SOD and catalase in the culture media. Samples from culture media were collected every 24 h, from CD3 until CD12 for 10 consecutive days. CrVI exponentially increased the levels of LPO from CD3 through CD12 (Fig. 6A). Compared to control, CrVI increased GPx activity on CD4, did not change on CD5, and decreased from CD6 to CD12 (Fig. 6B). CrVI did not change SOD activity on CD3 and CD4, however, CrVI significantly decreased SOD activity from CD5 to CD12 (Fig. 6C). CrVI significantly decreased catalase activity from CD3-CD12 (Fig. 6D).

Effects of CrVI on the expression of the cell cycle regulatory machinery

We determined mRNA expression of cell cycle regulatory genes on CD12 (that recapitulated PND4). CrVI significantly decreased *cyclin D2* and *D3*, *cyclins A1* and *A2*, and *cyclin B1* (Fig. 7). CrVI also down regulated cyclin-dependent kinase (*CDK*)*1* and *CDK2*, and up regulated *p27*. However, CrVI did not change *cyclin D1*, *E1*, *E2*, and *Cdk4*. We also determined cell survival machinery *Akt* and *Pcna*. CrVI down regulated both. Since many of the proteins are regulated post translationally, we determined the protein expression of the selective candidates from the above panel. Compared to control, CrVI down regulated pAKT (Fig. 8A-C). In control ovaries PCNA was highly expressed very specific to the

oocytes (Fig. 8D). On the other hand, CrVI decreased PCNA expression in the oocytes and increased PCNA in the granulosa cells (Fig. 8E). Control ovaries highly expressed cyclins A2 (Fig. 8G-I), B1 (Fig. 8J-L) and CDK1 (Fig. 8M-O), whereas, CrVI downregulated these proteins compared to control.

Discussion

Our results demonstrate that *in vitro* treatment with a low dose of CrVI (0.1 ppm) increased germ cell apoptosis, enhanced GCN breakdown, and advanced primordial follicle assembly by (i) increasing pro-apoptotic markers caspase 3, BAX, p53 and PUMA and down regulating BCL2; (ii) CrVI increased oxidative stress and decreased antioxidant enzymes GPx, SOD and catalase; (iii) CrVI significantly down regulated oocyte specific markers GDF9, BMP15 and cKIT; and (iv) CrVI decreased pAKT, PCNA, and cyclins and CDK1 that regulate M- and S-phases. We used an *in vitro* fetal whole ovarian model system that allowed easy manipulation with a view to histological and molecular parameters during early follicle development. This study describes the (i) characteristics of a 12 day *in vitro* whole fetal ovary culture system, which permits the survival and apoptosis of germ cells, and primordial follicle assembly that precedes GCN breakdown; (ii) it determines the effects of regulatory dose of CrVI on germ cell apoptosis, GCN breakdown and primordial follicle assembly; (iii) it compares the previous *in vitro* fetal whole ovarian culture model systems (Martinovitch, 1938; Blandau *et al.*, 1965; Motohashi *et al.*, 2009) and identifies the usefulness of adapting this unique model system to screen and assess the effects of CrVI on the ovarian development during the embryonic period.

Follicular development begins *in utero* with the transformation of primordial germ cells into oocytes (Hirshfield, 1997) that comprises various steps from the breaking down of GCN to the development of pre-ovulatory follicles. In rats, primordial follicles form during the postnatal days 3 and 4 (Gelety and Magoffin, 1997; Jones, 2012). One-third of the primordial follicles undergo rapid atresia within a few days after birth (Hirshfield and DeSanti, 1995; Hirshfield, 1997). Defects in either the timing or process of GCN breakdown can result in improper primordial follicle assembly and/or accelerated atresia, resulting in early reproductive senescence or infertility. Several EDCs are associated with POF (Diamanti-Kandarakis *et al.*, 2009; Gore *et al.*, 2011). While EDCs such as BPA and genistein delay GCN breakdown (Jefferson *et al.*, 2006; Zhou *et al.*, 2015) CrVI accelerates it (Sivakumar *et al.*, 2014) by altering the apoptotic machinery and/or disrupting collagen matrix by targeting Xpnpep2, a POF marker/candidate gene in POF women (Banu *et al.*, 2015). Detailed mechanisms pertaining to the effects of EDCs on germ cell death or GCN breakdown are lacking due to lack of screening tools. With thousands of environmental chemicals being registered every year, it is very difficult to evaluate or test these chemicals specific to ovotoxicity using *in vivo* models. Therefore, developing an *in vitro* fetal whole ovarian culture model system will allow us not only to screen and test such chemicals cost-effectively, but also to understand the mechanism at the molecular level.

BCL2 promotes cell survival by inhibiting caspases (Adams and Cory, 1998; Cory *et al.*, 2003). Over expression of BCL2 protein in the ovary leads to decreased ovarian somatic cell apoptosis, enhanced folliculogenesis, and increased susceptibility to ovarian germ cell

tumorigenesis in transgenic animals (Hsu *et al.*, 1996). Another study from human fetal ovarian tissue spanning the period between 12 and 38 gestational weeks indicated that the highest incidence of apoptotic germ cells coincide with the lack of detectable BCL2 protein (Albamonte *et al.*, 2008). In the current study, anti-apoptotic BCL2 is abundantly expressed in control ovaries and CrVI down regulated BCL2. This suggests that CrVI may have partly induced germ cell death and accelerated GCN breakdown by decreasing BCL2.

BAX is a regulator of germ cell death that controls the size of the primordial follicle pool (Felici *et al.*, 1999; Greenfeld *et al.*, 2007). BAX is upregulated in the ovaries during germ cell atresia and in fetal germ cells undergoing apoptosis (Felici *et al.*, 1999). *Bax*$^{-/-}$ females have prolonged reproductive longevity due to reduced atresia of immature follicles (Perez *et al.*, 1999). In the current study CrVI up regulated BAX expression in the ovaries on CD9. CrVI also significantly increased caspase 3 expression compared to control. Therefore, we suggest that CrVI may have increased germ cell apoptosis and accelerated GCN breakdown through a caspase 3-mediated mechanism downstream of BAX.

Our previous finding indicated that p53 plays a critical role in CrVI-induced granulosa cell apoptosis by altering sub-cellular localization of p53 and ERK1/2 in granulosa cells (Banu *et al.*, 2011). Interestingly, CrVI increased the co-localization of p53 with the antioxidant enzyme SOD2, thus inhibiting the scavenging of free radicals and increasing oxidative stress (Sivakumar *et al.*, 2014). In the current study, CrVI up regulated p53 compared to control. DNA damage-induced apoptosis of primordial follicle oocytes is mediated by the transcriptional activation of PUMA (Kerr *et al.*, 2012), highlighting an essential role for PUMA in the elimination of oocytes following genotoxic stress during meiotic arrest. Thus, PUMA, a potent cell killer belonging to the BH3-only subgroup of the BCL2 family, acts as a key regulator of the germ cell number and primordial follicle endowment in mice (Myers *et al.*, 2014). PUMA is the most important cell death regulator thus far identified in the female germ line mice (Myers *et al.*, 2014). CrVI significantly up regulated PUMA. It has been suggested in the mouse ovary that PUMA plays a critical role in apoptosis of primordial germ cells prior to meiotic entry, either during migration to the gonad or soon after their arrival (Myers *et al.*, 2014). Our current study shows that both p53 and its downstream candidate PUMA may play a critical role in CrVI-induced apoptosis of germ cells in PND1 ovaries, at the time of active GCN breakdown.

We further evaluated atresia of pre-antral (primordial and primary) follicles. Even though CrVI advanced primordial follicle assembly, it significantly increased primordial and primary follicle atresia and decreased expression of oocyte specific proteins GDF9, BMP15 and cKIT. GDF9 and BMP15 are known to increase granulosa cell proliferation (Juengel and McNatty, 2005). GDF9 can increase primordial and primary follicle numbers (Otsuka *et al.*, 2011). Furthermore, the blockage of cKIT signaling in oocytes by using a cKIT-neutralizing antibody markedly suppressed BMP15-induced granulosa cell mitosis, suggesting that the oocytes play a critical role in the granulosa cells responses to BMP15 (Otsuka and Shimasaki, 2002). In the human, combined mutations in BMP15 and GDF9 is associated with POF (Dixit *et al.*, 2005; Dixit *et al.*, 2006). PND4 is the initial period for the proliferation and differentiation of granulosa cells (Picut *et al.*, 2015). Our data from the current study showed that CrVI down regulated GDF9, BMP15 and cKIT. In addition CrVI

down regulated *cyclins (A1, A2, B1)* and *Cdk1* and *Cdk2*; and up regulated Cdk-inhibitor *p27*. While cyclins A1/A2 and CDK 2 regulate S-phase of the cell cycle, cyclin B1 and CDK1 regulate M-phase (Hochegger *et al.*, 2008). Interestingly, CrVI did not alter *cyclins D1*, *E1*, *E2* and *CDK4*, which are the major regulators of G1 phase. Therefore, it is suggested that CrVI may disrupt cell cycle during S- and M-phases. In addition, CrVI also down regulated cell survival machinery phospho-AKT. Interestingly, CrVI decreased PCNA in the oocytes and increased it in the granulosa cells. A number of studies have analyzed the post-translational modifications of PCNA and revealed its importance in the DNA damage response and maintenance of genomic integrity (Zhu *et al.*, 2014). Thus, the genome-wide roles of PCNA spans beyond cell survival (Paunesku *et al.*, 2001; Wang, 2014). The differential expression pattern of PCNA in the oocyte and granulosa cells in response to CrVI may be associated with its varying roles in both the cell types. Together, the data suggest that decrease in cell survival proteins and cell cycle machinery may partly contribute to the atresia of the pre-antral follicles which precede the apoptosis of granulosa cells and the oocytes.

Exposure to heavy metals, including CrVI during pregnancy increases oxidative stress (Flora *et al.*, 2011; Gundacker and Hengstschlager, 2012; Ni *et al.*, 2014), resulting in adverse pregnancy outcomes. In order to determine the contribution of oxidative stress in CrVI-induced apoptosis and follicle atresia, we estimated oxidative stress marker (LPO) and antioxidant enzyme activities (GPx, SOD and catalase) in the culture media every day from CD3-CD12. From CD3-12, CrVI increased LPO activity, and significantly decreased the activities of GPx, SOD and catalase. Together, it is suggested that oxidative stress (ROS)-p53(PUMA)-BAX-Caspase3 pathway may predominantly orchestrate germ cell death in the fetal ovary due to CrVI (Fig. 8). Interestingly, the current study has chosen a safety or regulatory dose of total Cr in the drinking water (USEPA, 2009), and found a significant impact on the germ cell death with a low dose. Therefore, the outcome of the study may be used to revisit the regulatory policies of CrVI content in the drinking water.

Our future studies will (i) identify the mechanisms of acute and sub-acute exposure to CrVI during prenatal ovarian development on germ cell apoptosis; and (ii) target these pathways to mitigate CrVI-induced germ cell apoptosis, or rescue germ cells from CrVI-induced cell death by using various specific inhibitors. To the best of our knowledge and based on the available literature, this is the first report in determining the role of (ROS)-p53-PUMA-BAX-Caspase3 pathway in regulating germ cell death, GCN breakdown and primordial follicle assembly in response to any heavy metal exposure in the fetal ovary using whole organ culture. Further research using this model is expected to emerge as a powerful tool for screening of various EDCs and testing the effects of drugs or inhibitors specific to germ cell death. In addition, our findings could help testing other heavy metal threats that may also underlie a developmental origin of later diseases, namely sub- or infertility from ovarian dysfunction.

Acknowledgements

This work was supported by National Institute of Environmental Health Sciences (NIEHS) grants ES020561-01 (S.K.B.) and the Center for Translational Environmental Health Research (CTEHR, P30ES023512) (S.K.B., R.C.B). Confocal microscopy was performed in the Texas A&M University College of Veterinary Medicine &

Biomedical Sciences Image Analysis Laboratory, supported by an NIH-NCRR Shared Instrumentation Grant (R.C.B.) (1 S10 RR22532-01). Authors gratefully acknowledge Dr. Patricia B. Hoyer, Department of Physiology, The University of Arizona Collage of Medicine, Tucson, for providing training in whole ovarian culture. We also acknowledge Dr. Rola Barhoumi, Department of Veterinary Integrative Biosciences, Texas A&M University, for the assistance with confocal microscopy. We acknowledge Kirthiram K. Sivakumar for performing a part of IHC and Thamizh K. Nithy for her assistance with figures.

References

Adams JM, Cory S. The Bcl-2 protein family: arbiters of cell survival. Science. 1998; 281:1322–1326. [PubMed: 9735050]

Albamonte MS, Willis MA, Albamonte MI, Jensen F, Espinosa MB, Vitullo AD. The developing human ovary: immunohistochemical analysis of germ-cell-specific VASA protein, BCL-2/BAX expression balance and apoptosis. Hum Reprod. 2008; 23:1895–1901. [PubMed: 18534994]

Armenti AE, Zama AM, Passantino L, Uzumcu M. Developmental methoxychlor exposure affects multiple reproductive parameters and ovarian folliculogenesis and gene expression in adult rats. Toxicology and Applied Pharmacology. 2008; 233:286–296. [PubMed: 18848953]

Banu SK, Stanley JA, Lee J, Stephen SD, Arosh JA, Hoyer PB, Burghardt RC. Hexavalent chromium-induced apoptosis of granulosa cells involves selective sub-cellular translocation of Bcl-2 members, ERK1/2 and p53. Toxicol Appl Pharmacol. 2011; 251:253–266. [PubMed: 21262251]

Banu SK, Stanley JA, Sivakumar KK, Arosh JA, Barhoumi R, Burghardt RC. Identifying a Novel Role for X-prolyl Aminopeptidase (Xpnpep) 2 in CrVI-Induced Adverse Effects on Germ Cell Nest Breakdown and Follicle Development in Rats. Biology of reproduction. 2015; 92:67. [PubMed: 25568306]

Blandau R, Warrick E, Rumery RE. In vitro cultivation of fetal mouse ovaries. Fertil Steril. 1965; 16:705–715. [PubMed: 5891577]

Borgeest C, Symonds D, Mayer LP, Hoyer PB, Flaws JA. Methoxychlor May Cause Ovarian Follicular Atresia and Proliferation of the Ovarian Epithelium in the Mouse. Toxicological Sciences. 2002; 68:473–478. [PubMed: 12151644]

Cory S, Huang DCS, Adams JM. The Bcl-2 family: roles in cell survival and oncogenesis. Oncogene. 2003; 22:8590–8607. [PubMed: 14634621]

Coucouvanis EC, Sherwood SW, Carswell-Crumpton C, Spack EG, Jones PP. Evidence that the mechanism of prenatal germ cell death in the mouse is apoptosis. Exp Cell Res. 1993; 209:238–247. [PubMed: 8262141]

de Boo HA, Harding JE. The developmental origins of adult disease (Barker) hypothesis. Aust N Z J Obstet Gynaecol. 2006; 46:4–14. [PubMed: 16441686]

Devine PJ, Sipes IG, Skinner MK, Hoyer PB. Characterization of a rat in vitro ovarian culture system to study the ovarian toxicant 4-vinylcyclohexene diepoxide. Toxicol Appl Pharmacol. 2002; 184:107–115. [PubMed: 12408955]

Diamanti-Kandarakis E, Bourguignon J-P, Giudice LC, Hauser R, Prins GS, Soto AM, Zoeller RT, Gore AC. Endocrine-Disrupting Chemicals: An Endocrine Society Scientific Statement. Endocrine Reviews. 2009; 30:293–342. [PubMed: 19502515]

Dixit H, Rao L, Padmalatha V, Kanakavalli M, Deenadayal M, Gupta N, Chakrabarty B, Singh L. Missense mutations in the BMP15 gene are associated with ovarian failure. Hum Genet. 2006; 119:408–415. [PubMed: 16508750]

Dixit H, Rao LK, Padmalatha V, Kanakavalli M, Deenadayal M, Gupta N, Chakravarty B, Singh L. Mutational screening of the coding region of growth differentiation factor 9 gene in Indian women with ovarian failure. Menopause. 2005; 12:749–754. [PubMed: 16278619]

Dong J, Albertini DF, Nishimori K, Kumar TR, Lu N, Matzuk MM. Growth differentiation factor-9 is required during early ovarian folliculogenesis. Nature. 1996; 383:531–535. [PubMed: 8849725]

Felici MD, Carlo AD, Pesce M, Iona S, Farrace MG, Piacentini M. Bcl-2 and Bax regulation of apoptosis in germ cells during prenatal oogenesis in the mouse embryo. Cell Death Differ. 1999; 6:908–915. [PubMed: 10510473]

Flora, SJS.; Pachauri, V.; Saxena, G. Chapter 33 - Arsenic, cadmium and lead. In: Gupta, RC., editor. Reproductive and Developmental Toxicology. Academic Press; San Diego: 2011. p. 415-438.

Gelety TJ, Magoffin DA. Ontogeny of steroidogenic enzyme gene expression in ovarian theca-interstitial cells in the rat: regulation by a paracrine theca-differentiating factor prior to achieving luteinizing hormone responsiveness. Biology of reproduction. 1997; 56:938–945. [PubMed: 9096876]

Giaccia AJ, Kastan MB. The complexity of p53 modulation: emerging patterns from divergent signals. Genes Dev. 1998; 12:2973–2983. [PubMed: 9765199]

Gore AC, Walker DM, Zama AM, Armenti AE, Uzumcu M. Early Life Exposure to Endocrine-Disrupting Chemicals Causes Lifelong Molecular Reprogramming of the Hypothalamus and Premature Reproductive Aging. Molecular Endocrinology. 2011; 25:2157–2168. [PubMed: 22016562]

Greenfeld CR, Babus JK, Furth PA, Marion S, Hoyer PB, Flaws JA. BAX is involved in regulating follicular growth, but is dispensable for follicle atresia in adult mouse ovaries. Reproduction (Cambridge, England). 2007; 133:107–116.

Gundacker C, Hengstschlager M. The role of the placenta in fetal exposure to heavy metals. Wien Med Wochenschr. 2012; 162:201–206. [PubMed: 22717874]

Haupt S, Berger M, Goldberg Z, Haupt Y. Apoptosis - the p53 network. J Cell Sci. 2003a; 116:4077–4085. [PubMed: 12972501]

Haupt S, Louria-Hayon I, Haupt Y. P53 licensed to kill? Operating the assassin. J Cell Biochem. 2003b; 88:76–82. [PubMed: 12461776]

Hemminki K, Kyyronen P, Niemi ML, Koskinen K, Sallmen M, Vainio H. Spontaneous abortions in an industrialized community in Finland. Am J Public Health. 1983; 73:32–37. [PubMed: 6847997]

Hemminki K, Niemi ML, Koskinen K, Vainio H. Spontaneous abortions among women employed in the metal industry in Finland. Int Arch Occup Environ Health. 1980; 47:53–60. [PubMed: 7429646]

Hirshfield AN. Overview of ovarian follicular development: Considerations for the toxicologist. Environmental and Molecular Mutagenesis. 1997; 29:10–15. [PubMed: 9020302]

Hirshfield AN, DeSanti AM. Patterns of ovarian cell proliferation in rats during the embryonic period and the first three weeks postpartum. Biology of reproduction. 1995; 53:1208–1221. [PubMed: 8527527]

Hochegger H, Takeda S, Hunt T. Cyclin-dependent kinases and cell-cycle transitions: does one fit all? Nat Rev Mol Cell Biol. 2008; 9:910–916. [PubMed: 18813291]

Hsu SY, Lai RJ, Finegold M, Hsueh AJ. Targeted overexpression of Bcl-2 in ovaries of transgenic mice leads to decreased follicle apoptosis, enhanced folliculogenesis, and increased germ cell tumorigenesis. Endocrinology. 1996; 137:4837–4843. [PubMed: 8895354]

Jefferson W, Newbold R, Padilla-Banks E, Pepling M. Neonatal genistein treatment alters ovarian differentiation in the mouse: inhibition of oocyte nest breakdown and increased oocyte survival. Biology of reproduction. 2006; 74:161–168. [PubMed: 16192398]

Jones, RL. Molecular Mechanisms Regulating Neonatal Oocyte Survival and Primordial Follicle Formation in the Mouse Ovary, Biology. Syracuse University; Syracuse, NY: 2012. p. 1-121.

Juengel JL, McNatty KP. The role of proteins of the transforming growth factor-beta superfamily in the intraovarian regulation of follicular development. Hum Reprod Update. 2005; 11:143–160. [PubMed: 15705960]

Kerr JB, Hutt KJ, Michalak EM, Cook M, Vandenberg CJ, Liew SH, Bouillet P, Mills A, Scott CL, Findlay JK, Strasser A. DNA damage-induced primordial follicle oocyte apoptosis and loss of fertility require TAp63-mediated induction of Puma and Noxa. Mol Cell. 2012; 48:343–352. [PubMed: 23000175]

Leary, S.; Underwood, W.; Anthony, R.; Cartner, S.; Corey, D.; Grandin, T.; Greenacre, CB.; Gwaltney-Bran, S.; McCrackin, MA.; Meyer, R. AVMA guidelines for the euthanasia of animals: 2013 edition. American Veterinary Medical Association; Schaumburg, IL: 2013. p. 46-50.

Li Y, Xu X, Liu J, Wu K, Gu C, Shao G, Chen S, Chen G, Huo X. The hazard of chromium exposure to neonates in Guiyu of China. Sci Total Environ. 2008; 403:99–104. [PubMed: 18603282]

Maeng SH, Chung HW, Kim KJ, Lee BM, Shin YC, Kim SJ, Yu IJ. Chromosome aberration and lipid peroxidation in chromium-exposed workers. Biomarkers. 2004; 9:418–434. [PubMed: 15849063]

Manikkam M, Haque MM, Guerrero-Bosagna C, Nilsson EE, Skinner MK. Pesticide methoxychlor promotes the epigenetic transgenerational inheritance of adult-onset disease through the female germline. PloS one. 2014; 9:e102091. [PubMed: 25057798]

Martinovitch PN. The Development in vitro of the Mammalian Gonad. Ovary and Ovogenesis. Proceedings of the Royal Society of London. Series B, Biological Sciences. 1938; 125:232–249.

Motohashi HH, Sankai T, Nariai K, Sato K, Kada H. Effects of in vitro culture of mouse fetal gonads on subsequent ovarian development in vivo and oocyte maturation in vitro. Hum Cell. 2009; 22:43–48. [PubMed: 19379463]

Myers M, Morgan FH, Liew SH, Zerafa N, Gamage TU, Sarraj M, Cook M, Kapic I, Sutherland A, Scott CL, Strasser A, Findlay JK, Kerr JB, Hutt KJ. PUMA regulates germ cell loss and primordial follicle endowment in mice. Reproduction (Cambridge, England). 2014; 148:211–219.

Ni W, Huang Y, Wang X, Zhang J, Wu K. Associations of neonatal lead, cadmium, chromium and nickel co-exposure with DNA oxidative damage in an electronic waste recycling town. Sci Total Environ. 2014; 472:354–362. [PubMed: 24295751]

Nilsson E, Larsen G, Manikkam M, Guerrero-Bosagna C, Savenkova MI, Skinner MK. Environmentally induced epigenetic transgenerational inheritance of ovarian disease. PloS one. 2012; 7:e36129. [PubMed: 22570695]

Orisaka M, Orisaka S, Jiang JY, Craig J, Wang Y, Kotsuji F, Tsang BK. Growth differentiation factor 9 is antiapoptotic during follicular development from preantral to early antral stage. Mol Endocrinol. 2006; 20:2456–2468. [PubMed: 16740654]

Osman P. Rate and course of atresia during follicular development in the adult cyclic rat. Journal of Reproduction and Fertility. 1985; 73:261–270. [PubMed: 4038517]

Otsuka F, McTavish KJ, Shimasaki S. Integral role of GDF-9 and BMP-15 in ovarian function. Mol Reprod Dev. 2011; 78:9–21. [PubMed: 21226076]

Otsuka F, Shimasaki S. A negative feedback system between oocyte bone morphogenetic protein 15 and granulosa cell kit ligand: its role in regulating granulosa cell mitosis. Proc Natl Acad Sci U S A. 2002; 99:8060–8065. [PubMed: 12048244]

Paunesku T, Mittal S, Protic M, Oryhon J, Korolev SV, Joachimiak A, Woloschak GE. Proliferating cell nuclear antigen (PCNA): ringmaster of the genome. Int J Radiat Biol. 2001; 77:1007–1021. [PubMed: 11682006]

Pepling ME. From primordial germ cell to primordial follicle: mammalian female germ cell development. Genesis. 2006; 44:622–632. [PubMed: 17146778]

Pepling ME, Spradling AC. Female mouse germ cells form synchronously dividing cysts. Development. 1998; 125:3323–3328. [PubMed: 9693136]

Pepling ME, Spradling AC. Mouse Ovarian Germ Cell Cysts Undergo Programmed Breakdown to Form Primordial Follicles. Developmental Biology. 2001; 234:339–351. [PubMed: 11397004]

Perez GI, Robles R, Knudson CM, Flaws JA, Korsmeyer SJ, Tilly JL. Prolongation of ovarian lifespan into advanced chronological age by Bax-deficiency. Nat Genet. 1999; 21:200–203. [PubMed: 9988273]

Picut CA, Dixon D, Simons ML, Stump DG, Parker GA, Remick AK. Postnatal ovary development in the rat: morphologic study and correlation of morphology to neuroendocrine parameters. Toxicol Pathol. 2015; 43:343–353. [PubMed: 25107574]

Prueitt RL, Ross JL, Zinn AR. Physical mapping of nine Xq translocation breakpoints and identification of XPNPEP2 as a premature ovarian failure candidate gene. Cytogenetics and cell genetics. 2000; 89:44–50. [PubMed: 10894934]

Quansah R, Jaakkola JJ. Paternal and maternal exposure to welding fumes and metal dusts or fumes and adverse pregnancy outcomes. Int Arch Occup Environ Health. 2009; 82:529–537. [PubMed: 18820944]

Rajah R, Glaser EM, Hirshfield AN. The changing architecture of the neonatal rat ovary during histogenesis. Dev Dyn. 1992; 194:177–192. [PubMed: 1467554]

Ratts VS, Flaws JA, Kolp R, Sorenson CM, Tilly JL. Ablation of bcl-2 gene expression decreases the numbers of oocytes and primordial follicles established in the post-natal female mouse gonad. Endocrinology. 1995; 136:3665–3668. [PubMed: 7628407]

Rivera OE, Varayoud J, Rodríguez HA, Muñoz-de-Toro M, Luque EH. Neonatal exposure to bisphenol A or diethylstilbestrol alters the ovarian follicular dynamics in the lamb. Reproductive Toxicology. 2011; 32:304–312. [PubMed: 21722727]

Rodríguez HA, Santambrosio N, Santamaría CG, Muñoz-de-Toro M, Luque EH. Neonatal exposure to bisphenol A reduces the pool of primordial follicles in the rat ovary. Reproductive Toxicology. 2010; 30:550–557. [PubMed: 20692330]

Sawyer HR, Smith P, Heath DA, Juengel JL, Wakefield SJ, McNatty KP. Formation of ovarian follicles during fetal development in sheep. Biology of reproduction. 2002; 66:1134–1150. [PubMed: 11906935]

Schmittgen TD, Livak KJ. Analyzing real-time PCR data by the comparative CT method. Nat. Protocols. 2008; 3:1101–1108. [PubMed: 18546601]

Shi Z, Valdez KE, Ting AY, Franczak A, Gum SL, Petroff BK. Ovarian endocrine disruption underlies premature reproductive senescence following environmentally relevant chronic exposure to the aryl hydrocarbon receptor agonist 2, 3, 7, 8-tetrachlorodibenzo-p-dioxin. Biology of reproduction. 2007; 76:198–202. [PubMed: 17050859]

Shmitova LA. Content of hexavalent chromium in the biological substrates of pregnant women and puerperae engaged in the manufacture of chromium compounds. Gig Tr Prof Zabol. 1980:33–35. [PubMed: 7372143]

Sivakumar KK, Stanley JA, Arosh JA, Pepling ME, Burghardt RC, Banu SK. Prenatal exposure to chromium induces early reproductive senescence by increasing germ cell apoptosis and advancing germ cell cyst breakdown in the F1 offspring. Dev Biol. 2014; 388:22–34. [PubMed: 24530425]

Stanley JA, Sivakumar KK, Arosh JA, Burghardt RC, Banu SK. Edaravone mitigates hexavalent chromium-induced oxidative stress and depletion of antioxidant enzymes while estrogen restores antioxidant enzymes in the rat ovary in F1 offspring. Biology of reproduction. 2014; 91:12. [PubMed: 24804965]

Stanley JA, Sivakumar KK, Nithy TK, Arosh JA, Hoyer PB, Burghardt RC, Banu SK. Postnatal exposure to chromium through mother's milk accelerates follicular atresia in F1 offspring through increased oxidative stress and depletion of antioxidant enzymes. Free Radic Biol Med. 2013; 61C: 179–196. [PubMed: 23470461]

Stern RM, Berlin A, Fletcher A, Hemminki K, Jarvisalo J, Peto J. International conference on health hazards and biological effects of welding fumes and gases. International Archives of Occupational and Environmental Health. 1986; 57:237–246.

Tawfik H, Kline J, Jacobson J, Tehranifar P, Protacio A, Flom JD, Cirillo P, Cohn BA, Terry MB. Life course exposure to smoke and early menopause and menopausal transition. Menopause. 2015

Thomas FH, Vanderhyden BC. Oocyte-granulosa cell interactions during mouse follicular development: regulation of kit ligand expression and its role in oocyte growth. Reprod Biol Endocrinol. 2006; 4:1–8. [PubMed: 16436209]

USEPA. National primary drinking water regulations, EPA 816-F-09-004. United States Environmental Protection Agency; Washington, D.C.: 2009. p. 1-6.

Wang SC. PCNA: a silent housekeeper or a potential therapeutic target? Trends Pharmacol Sci. 2014; 35:178–186. [PubMed: 24655521]

Wang W, Hafner KS, Flaws JA. In utero bisphenol A exposure disrupts germ cell nest breakdown and reduces fertility with age in the mouse. Toxicol Appl Pharmacol. 2014; 276:157–164. [PubMed: 24576723]

Yamakuchi M, Lowenstein CJ. MiR-34, SIRT1 and p53: the feedback loop. Cell Cycle. 2009; 8:712–715. [PubMed: 19221490]

Yan C, Wang P, DeMayo J, DeMayo FJ, Elvin JA, Carino C, Prasad SV, Skinner SS, Dunbar BS, Dube JL, Celeste AJ, Matzuk MM. Synergistic Roles of Bone Morphogenetic Protein 15 and Growth Differentiation Factor 9 in Ovarian Function. Molecular Endocrinology. 2001; 15:854–866. [PubMed: 11376106]

Yang Y, Liu H, Xiang XH, Liu FY. Outline of occupational chromium poisoning in China. Bull Environ Contam Toxicol. 2013; 90:742–749. [PubMed: 23604023]

Zhou C, Wang W, Peretz J, Flaws JA. Bisphenol A exposure inhibits germ cell nest breakdown by reducing apoptosis in cultured neonatal mouse ovaries. Reprod Toxicol. 2015

Zhu Q, Chang Y, Yang JIN, Wei Q. Post-translational modifications of proliferating cell nuclear antigen: A key signal integrator for DNA damage response (Review). Oncology Letters. 2014; 7:1363–1369. [PubMed: 24765138]

Highlights

- CrVI (0.1 ppm, a regulatory dose) increased germ cell apoptosis of fetal ovaries.
- CrVI (0.1 ppm) increased pro-apoptotic proteins.
- CrVI (0.1 ppm) decreased cyclins and CDK1 and cell survival proteins.
- CrVI (0.1 ppm) increased oxidative stress during fetal ovarian development.
- We propose fetal ovarian culture model for high-throughput testing of heavy-metals.

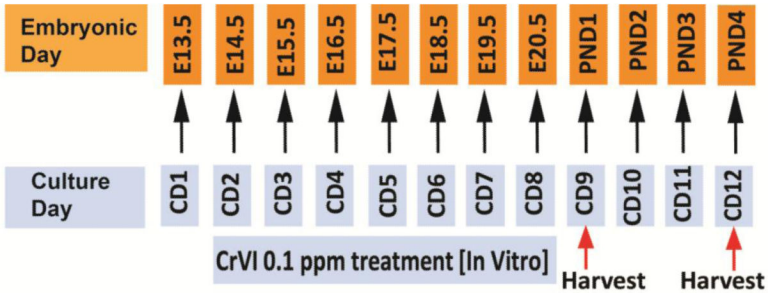

Fig. 1.

Experimental design for treatment with CrVI (0.1 ppm) *in vitro*. Embryonic/fetal ovaries were removed from normal pregnant dams on gestational day 13.5 and cultured for 12 days. Embryonic day (E) 13.5 was considered as culture day (CD) 1, and CD12 recapitulates postnatal day 4 as given in the schematic diagram. CrVI (0.1 ppm potassium dichromate) was added in the media on CD2 and media was changed every 24h and CrVI was freshly added every day for 7 days. Ovaries were harvested on CD9 and CD12, which recapitulates postnatal days 1 and 4, respectively.

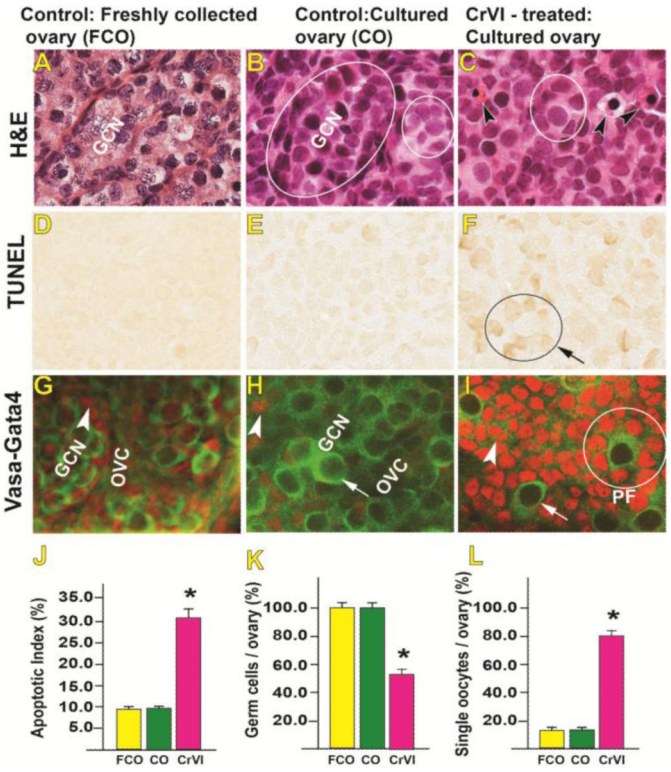

Fig. 2.

Effects of CrVI on germ cell/oocyte apoptosis in cultured whole fetal ovaries on culture day 9. Fetal whole ovaries from embryonic day (E) 13.5 were cultured for 8 days *in vitro*, and treated with CrVI (0.1 ppm) from CD2 to CD8, harvested on CD9 (which recapitulated PND1), and used for histology (A-C) or TUNEL (D-F) or double immunolabeling of whole mount ovaries (G-I). The apoptosis index (AI) was calculated as the average percentage of TUNEL-positive germ cells/oocytes from 10 ovaries. Average number of TUNEL-positive cells in control group was considered as 10%. *: control vs CrVI, $p<0.05$. Each value represents mean ± SEM of TUNEL-positive germ cells/oocytes counted from 15 fields. The width of field for each image is 220 or 350 μm. In Fig 2C, arrow heads point out pyknotic nuclei and circle indicates primary follicle; in Fig 2F, arrow points out a primary follicle with TUNEL-positive (apoptotic) granulosa cells. In Figs 2G-I, arrow heads point out granulosa cells (red) and arrows point out germ cells or oocytes (green). GCN – germ cell nest, OVC - ovigerous cord, PF-primary follicle. FCO – freshly collected ovaries from PND1, CO – cultured ovaries on CD9. Representative images and histograms are shown.

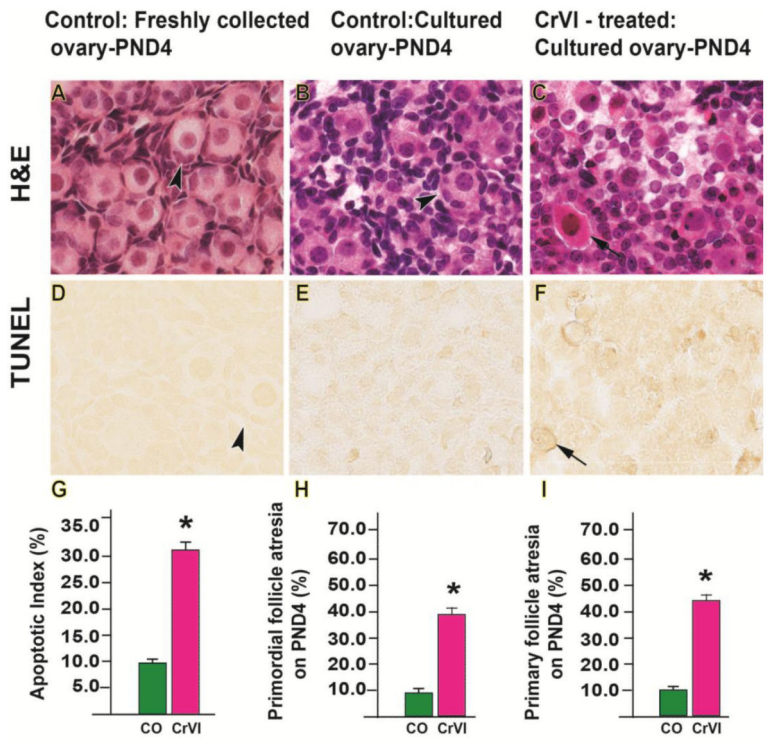

Fig. 3.

Effects of CrVI on follicle atresia in cultured whole fetal ovaries on culture day 12. Fetal ovaries from embryonic day (E) 13.5 were cultured for 11 days *in vitro*, and treated with CrVI (0.1 ppm) from CD2 to CD8, and harvested on CD12 (which recapitulated PND4). Ovaries from culture were harvested and fixed in 4% buffered paraformaldehyde and processed for histology (A-C) or in situ TUNEL apoptotic assay (D-F). The apoptosis index (AI) was calculated as the average percentage of TUNEL-positive oocytes from 10 ovaries. Average number of TUNEL-positive cells in control group was considered as 10%. Number of atretic primordial or primary follicles were counted in serial sections and expressed in percentage. *: control vs CrVI, $p<0.05$. The width of field for each image is 220 or 350 μm. Arrow heads point out healthy follicles. Arrows point out atretic follicles. Representative images and histograms are shown.

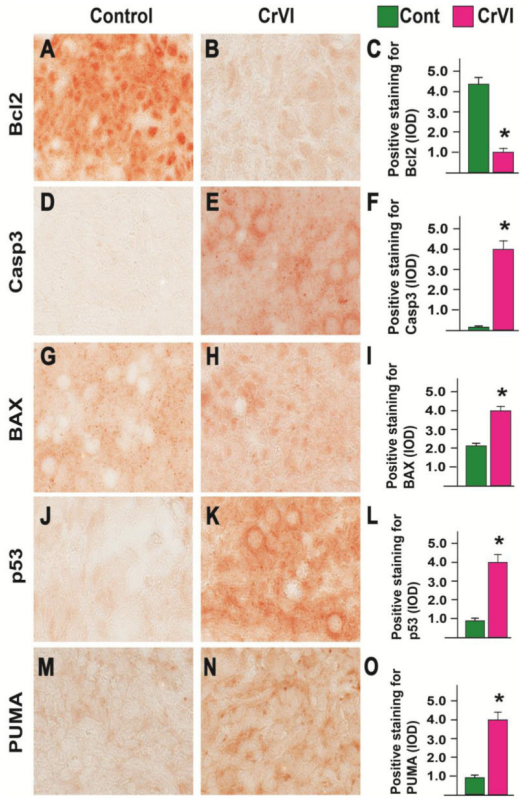

Fig. 4.

Effects of CrVI on the expression of BCL2, caspase3, BAX, p53 and PUMA in cultured whole fetal ovaries on culture day 9. Fetal ovaries from embryonic day (E) 13.5 were cultured for 8 days *in vitro* and treated with CrVI (0.1 ppm) from CD2 to CD8, and harvested on CD9 (which recapitulated PND1). Ovaries from culture were harvested and fixed in 4% buffered paraformaldehyde and processed for IHC. Integrated Optical Density (IOD) of staining was quantified using Image ProPlus software. The width of field for each image is 220 or 350 μm; BCL2 (A-C), caspase 3 (D-F), BAX (G-I), p53 (J-L) and PUMA (M-O). *: Control vs CrVI, $p<0.05$. Each value represents mean ± SEM of 10 ovaries. Representative images and histograms are shown.

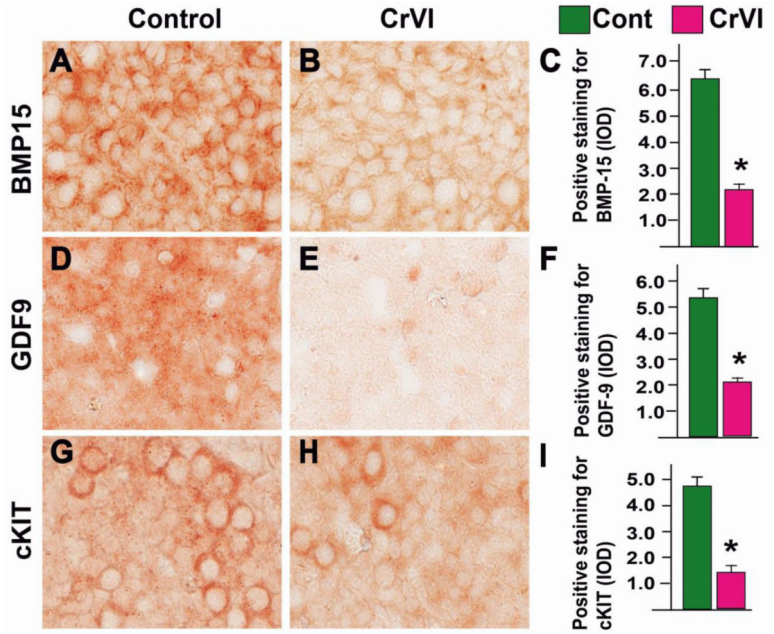

Fig. 5.

Effects of CrVI on the expression of BMP15, GDF9 and cKIT in cultured whole fetal ovaries on culture day 9. Fetal ovaries from embryonic day (E) 13.5 were cultured for 8 days *in vitro* and treated with CrVI (0.1 ppm) from CD2 to CD8, and harvested on CD9 (which recapitulated PND1). Ovaries from culture were harvested and fixed in 4% buffered paraformaldehyde and processed for IHC. Integrated Optical Density (IOD) of staining was quantified using Image ProPlus software. The width of field for each image is 220 or 350 μm; BMP15 (A-C), GDF9 (D-F), and cKIT (G-I). *: Control vs CrVI, $p<0.05$. Each value represents mean ± SEM of 10 ovaries. Representative images and histograms are shown.

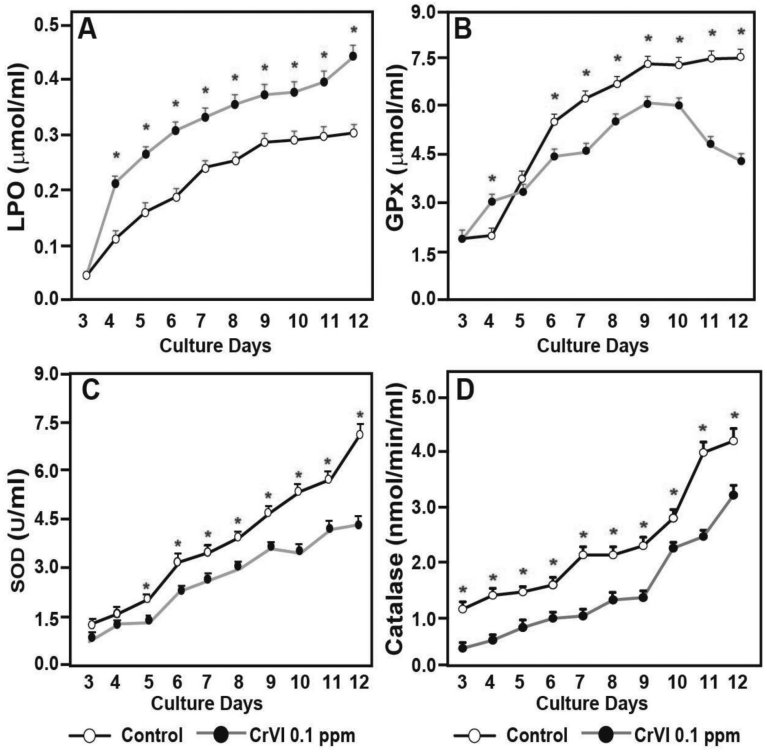

Fig. 6.

Effects of CrVI on the activities of lipid peroxidase (LPO) (A) and antioxidants GPx (B), SOD (C) and Catalase (D) in cultured whole fetal ovaries. Whole fetal ovaries from embryonic day (E) 13.5 were cultured for 12 days *in vitro*, and treated with CrVI (0.1 ppm) from CD2 to CD8. Culture media was collected every day from CD 3 to CD 12 and LPO, GPx, SOD and catalase activities were measured. *: Control vs CrVI, $p<0.05$. Each value represents mean ± SEM of 3 experiments.

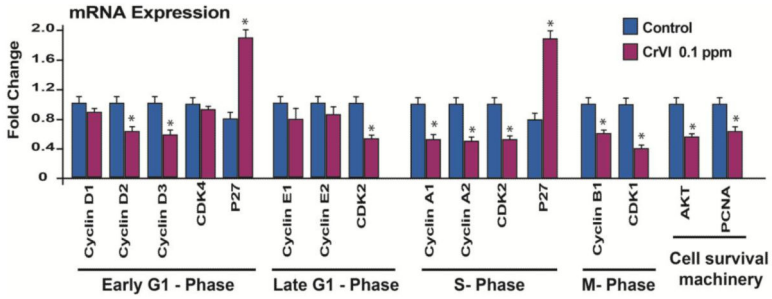

Fig. 7.

Effects of CrVI on the mRNA expression analysis of cell cycle regulatory machinery genes in cultured whole fetal ovaries on culture day 12. Fetal ovaries from embryonic day (E) 13.5 were cultured *in vitro*, and treated with CrVI (0.1 ppm) from CD2 to CD8, and harvested on CD12 (which recapitulated PND4). Ovaries from culture were harvested and mRNA expression of cell cycle regulatory machinery was analyzed by real time PCR. *: Control vs CrVI, $p<0.05$. Each value represents mean ± SEM of 3 experiments. Each sample was pooled from 5-8 ovaries.

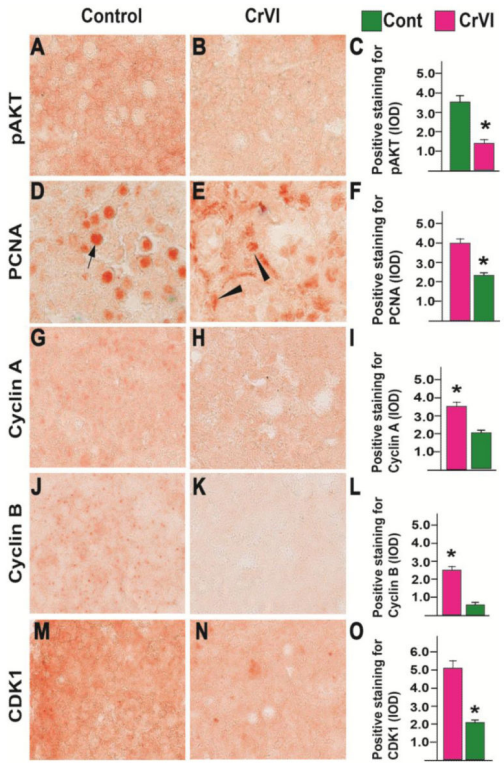

Fig. 8.

Effects of CrVI on the expression of phosphorylated (p) AKT, caspase 3, PCNA, cyclin A, cyclin B and CDK1 in cultured whole fetal ovaries on culture day 12. Fetal ovaries from embryonic day (E) 13.5 were cultured for 12 days *in vitro* and treated with CrVI (0.1 ppm) from CD2 to CD8, and harvested on CD12 (which recapitulated PND4). Ovaries from culture were harvested and fixed in 4% buffered paraformaldehyde and processed for IHC. Integrated Optical Density (IOD) of staining was quantified using Image ProPlus software. The width of field for each image is 220 or 350 μm; pAKT (A-C), PCNA (D-F), cyclin A (G-I), cyclin B (J-L) and CDK1 (M-O). *: Control vs CrVI, $p<0.05$. Each value represents mean ± SEM of 10 ovaries. Representative images and histograms are shown.

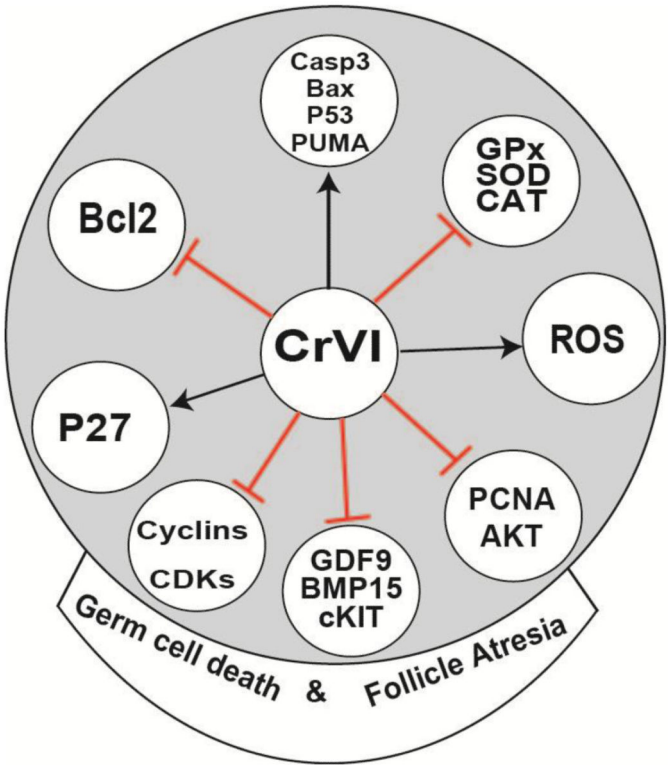

Fig. 9.

Schematic diagram depicting the possible mechanisms involved in CrVI-induced germ cell apoptosis and follicle atresia. Arrows indicate stimulatory response and bars (T) indicate inhibitory response.

Table 1

Sources of antibodies, catalog numbers, dilutions, host species, immunogens, and homologies with rat/mouse.

S.No.	Antibody	Company & Cat. No.	Dilution	Host Species	Immunogen	% of homology with rat and mouse	Secondary antibody	Dilution	Application
1	BCL2	Abcam; AB7973	1:300	Rabbit	Human	Rat: 100%; mouse: 100%	Goat anti-rabbit	1:200	IHC
2	BAX	Sigma: SAB4502549	1:1500	Rabbit	Human	Rat: 93%; mouse: 94%	Goat anti-rabbit	1:200	IHC
3	P53	Abcam; AB131442	1:500	Rabbit	Human	Rat: 100%; mouse: 100%	Goat anti-rabbit	1:200	IHC
4	PUMA	Abcam; AB9643	1:1000	Rabbit	Human	Rat: 79%; mouse: 79%	Goat anti-rabbit	1:200	IHC
5	BMP15	Abcam; AB108413	1:3000	Rabbit	Human	Rat: 94%; mouse: 94%	Goat anti-rabbit	1:200	IHC
6	cKIT	Sigma: SAB4300489	1:4000	Rabbit	Human	Rat: 100%; mouse: 100%	Goat anti-rabbit	1:200	IHC
7	GDF9	Abcam; AB93892	1:500	Rabbit	Human	Rat: 93%; mouse: 93%	Goat anti-rabbit	1:200	IHC
8	Cleaved-Caspase-3	Cell Signaling; 9661	1:100	Rabbit	Human	Rat: 100%; mouse: 100%	Goat anti-rabbit	1:200	IHC
9	Cyclin D2	Abcam: AB94685	1:50	Rabbit	Human	Rat: 100%; mouse: 100%	Goat anti-rabbit	1:200	IHC
10	Cyclin A2	Cell Signaling: 4656	1:100	Mouse	Human	Rat: 91%; mouse: 92%	Horse anti-mouse	1:200	IHC
11	Cyclin B1	Cell Signaling: 4138	1:100	Rabbit	Human	Rat: 90%; mouse: 90%	Goat anti-rabbit	1:200	IHC
12	CDK1	Cell Signaling: 9116	1:50	Mouse	Human	Rat: 90%; mouse: 90%	Horse anti-mouse	1:200	IHC
13	p-AKT	Cell Signaling: 3787	1:50	Rabbit	Mouse	Rat: 100%; mouse: 100%	Goat anti-rabbit	1:200	IHC
14	PCNA	Cell Signaling: 2586	1:250	Mouse	Rat	Rat: 100%; mouse: 100%	Horse anti-mouse	1:200	IHC
15	VASA	Abcam; AB13840	1:100	Rabbit polyclonal	Human	Rat: 95%; mouse: 98%	Goat anti-mouse Alexa 488 green	1:200	Immuno-colocalization

S.No.	Antibody	Company & Cat. No.	Dilution	Host Species	Immunogen	% of homology with rat and mouse	Secondary antibody	Dilution	Application
16	GATA-4	Santa Cruz; SC25310	1:50	Mouse Monoclonal	Human	Rat: 75%; mouse: 77%	Goat Anti-mouse 594 Red	1:200	Immuno-colocalization

Table 2

Oligonucleotide primers used.

Cyclin A1_*Forward*	5'-TGC AAA TGG GCA GTA CAG GAG GAC -3'
Cyclin A1_*Reverse*	5'- TCC ACC AGC CAG TCC ACC AGA ATC -3'
Cyclin A2_ *Forward*	5'- GAC GGG TTG CAC CCC TTA AGG ATG -3'
Cyclin A2_ *Reverse*	5'- GTT CAC AGC CAA ATG CAG GGT CTC -3'
Cyclin B1_ *Forward*	5'- CTG CTG CAG GAG ACC ATG TA -3'
Cyclin B1_ *Reverse*	5'- CTG TCT GAT CTG GTG CTT GG -3'
Cyclin D1_ *Forward*	5'- AAG GTT TAG GGC CAT GTG TG -3'
Cyclin D1_ *Reverse*	5'- GCA AGA ATG TGC CAG ACT CA -3'
Cyclin D2_ *Forward*	5'- CTA GCC CCT TCT CTC TCT CTC TCT A -3'
Cyclin D2_ *Reverse*	5'- CTA GTC TGA GGG CTC TCC TGT AAG -3'
Cyclin D3_ *Forward*	5'- GTC TTG AGG GTG CTG ATG GT -3'
Cyclin D3_ *Reverse*	5'- GAA GAT GAG CTG GAG GGC TA -3'
Cyclin E1_ *Forward*	5'- GAA TGA CCA GAC CTG CCA TC -3'
Cyclin E1_ *Reverse*	5'- GGC TGG TGT ACT CGA CCC TA -3'
Cyclin E2_ *Forward*	5'- CAT TCT GAC TTG GAA CCA CAG ATG -3'
Cyclin E2_ *Reverse*	5'- AAA TGG CAC AAG GCA GCA GCA GTC -3'
P27_ *Forward*	5'- GCC TGG CTC TAC TCC ACT TG -3'
P27_ *Reverse*	5'- GGG CTC CCG TTA GAC ACT CT -3'
CDK 1_ *Forward*	5'- AGG GAC CAT ATT TGC AGA GC -3'
CDK 1_ *Reverse*	5'- TCA TCC AGG TTC TTG ACG TG -3'
CDK 2_ *Forward*	5'- GCA CTT AAC CCG ACT TCC AG -3'
CDK 2_ *Reverse*	5'- TCC CAA CTT AGG CTT CTG CT -3'
CDK 4_ *Forward*	5'- TAC ATA TGC AAC GCC TGT GG -3'
CDK 4_ *Reverse*	5'- GGA AGG CAG AGA TTC GCT TA -3'
β-Actin_ *Forward*	5'- CAA CCT TCT TGC AGC TCC TC -3'
β-Actin_ *Reverse*	5'- TTC TGA CCC ATA CCC ACC AT -3'